Rev. Adv. Mater. Sci. 34 (2013) 1-11

MECHANICAL PROPERTIES OF GRAPHENE

I.A. Ovid'ko[1,2]

[1]Institute of Problems of Mechanical Engineering, Russian Academy of Sciences,
Bolshoj 61, Vasilievskii Ostrov, St. Petersburg 199178, Russia
[2]Department of Mathematics and Mechanics, St. Petersburg State University, St. Petersburg 198504, Russia

Received: February 01, 2013

Abstract. This article briefly summarizes the information now available, from recent experiments, computer simulations and theoretical models, addressing the outstanding mechanical properties of graphene. In particular, experimental data on superior strength and extremely high in-plane stiffness of pristine graphene are presented. The role of dislocations as carriers of plastic flow in graphene is discussed. Special attention is devoted to the effects of grain boundaries in polycrystalline graphene on its strength. Also, enhancement of fracture toughness due to graphene inclusions in nanocomposites is considered. Finally, important unsolved problems in interdisciplinary fundamental science and applied research of the mechanical properties exhibited by graphene are outlined.

1. INTRODUCTION

Graphene, a monolayer of covalently bonded carbon atoms, represents a new two-dimensional (2D) material having the unique mechanical and transport properties desired for a wide range of technologies; see, e.g., [1-4]. In particular, graphene shows the outstanding electron transport properties due to its 2D hexagonal crystal structure and the presence of charge carriers behaving like massless particles [2-4]. In addition, graphene is specified by extremely high in-plane stiffness - Young modulus - and superior (highest ever measured) strength [3,5]. The exceptional mechanical properties of graphene are of utmost importance for its applications, because they are highly needed (i) to exploit graphene as a superstrong structural material; (ii) to understand and control durability of graphene used in electronics and energy storage; (iii) to plastically form curved graphene specimens for electronics and structural applications; (iv) to exploit nanocomposites with graphene inclusions as structural and/or functional materials. Also, knowledge on micromechanisms of unique deformation and fracture processes in graphene is of crucial significance in fundamental science.

The remarkable electronic and mechanical properties of graphene represent the subjects of explosively growing research efforts whose trends and key results are highly interesting for systematic presentations in the form of reviews. Recently, the electronic properties of graphene have been considered in detail in the review [4] (cited over 3,000 times). The main aim of this paper is to give a brief overview of recent experiments, computer simulations and theoretical models, addressing the unique mechanical properties of graphene and nanocomposites containing graphene inclusions.

2. MECHANICAL PROPERTIES OF PRISTINE GRAPHENE

Pristine graphene structures represent 2D plane sheets of covalently bonded carbon atoms that form ideal hexagonal crystal lattices. Graphene specimens typically exist as either monolayers

Corresponding author: I.A. Ovid'ko, e-mail: ovidko@nano.ipme.ru

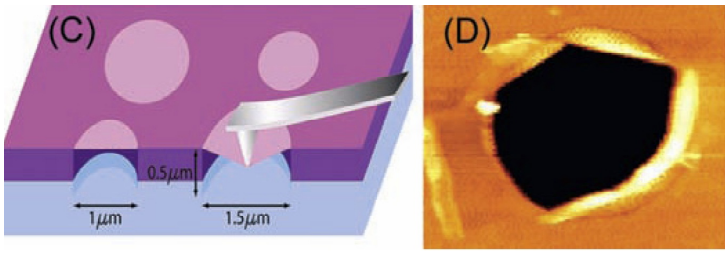

Fig. 1. Mechanical testing of graphene. Schematic of nanoindentation on suspended graphene membrane (left figure). Atomic force microscope image of a fractured graphene membrane (right figure). Reprinted with permission from [C. Lee, X. Wei, J.W. Kysar, J. Hone, *Science*, Volume 321, 385-388 (2008)]. Copyright (2008) by the American Association for the Advancement of Science.

attached to substrates made of another material (mostly SiC or a metal) or free-standing sheets. Following [3], the term "free-standing graphene" means that a graphene sheet is sufficiently isolated from its environment.

In general, mechanical properties of a crystalline solid are controlled by characteristics of its pristine crystal lattice and structural defects like dislocations and grain boundaries [6,7]. For instance, atom-atom interactions in the ideal, defect-free crystal lattice as well as lattice geometry cause elastic properties of a solid, whereas its strength and plastic flow stress are also strongly affected by characteristics of defects. Say, pre-existent defects dramatically decrease strength of real solids under mechanical load, compared to the ideal strength inherent to their counterparts free from defects. Structural defects are always present in conventional macroscale solids, and thereby their crucial influence on mechanical properties of these solids is inevitable. In nanoscale solids, however, defects can be absent in the initial, non-deformed state due to nanoscale and free-surface effects, and therefore such solids can exhibit superior strength close to its ideal highest value [8]. In particular, it is the case of comparatively small graphene sheets/membranes that can be fabricated in their pristine, defect-free state.

The first systematic experimental analysis of elastic properties and strength exhibited by pristine graphene has been done by Lee with co-workers [5]. In this experiment, a graphene membrane was mechanically deposited onto a substrate with arrays of circular wells and loaded by tip of atomic force microscope (Fig. 1); for details, see [5]. It was experimentally found that the graphene shows both non-linear elastic behavior and brittle fracture. The non-linear elastic response of graphene to tensile load is described as: $\sigma = E\varepsilon + D\varepsilon^2$, where σ is the applied stress (the symmetric second Piola-Kirchhoff stress), ε is the elastic strain (uniaxial Lagrangian strain), E is the Young modulus, and D is the third-order elastic stiffness. According to the experiment [5], graphene is characterized by Young modulus of E = 1.0 TPa and the third-order elastic stiffness of D = -2.0 TPa. The former value is extremely large and close to that specifying carbon nanotubes.

Brittle fracture of graphene occurs at a critical stress equal to its intrinsic strength of σ_{int} = 130 GPa [5]. This value is highest ever measured for real materials.

The discussed experimental data on the Young modulus (E = 1 TPa) and the intrinsic strength (σ_{int} = 130 GPa) exhibited by pristine graphene are consistent with computer simulations [9] showing values of E = 1.05 TPa and σ_{int} = 110 GPa. These values of E and σ_{int} are extremely large and make graphene to be very attractive for structural and other applications. At the same time, graphene can be easily bent, and this is also its specific behavioral feature that can be exploited in practice.

Crystallographic characteristics of crack growth in monolayer graphene have been examined in both experiment and molecular dynamics simulations [10]. It was experimentally revealed that cracks or, in other terms, tears are generated and grow in suspended monolayer graphene membranes under unavoidable mechanically applied stress during their processing. In doing so, tears grow predominantly along straight lines – in either the armchair or zigzag directions of the hexagonal crystal lattice of graphene - occasionally changing growth direction by 30° (Fig. 2). In addition, tears generated under mechanical load in suspended graphene membranes sometimes can grow under TEM electron beam [10]. Kim and coworkers [10] treat this growth process to be driven by a combination of high local stresses concentrated near tear tips and ionization effects of electron beam. In this situation, simultaneously strained and electron-beam excited atomic bonds

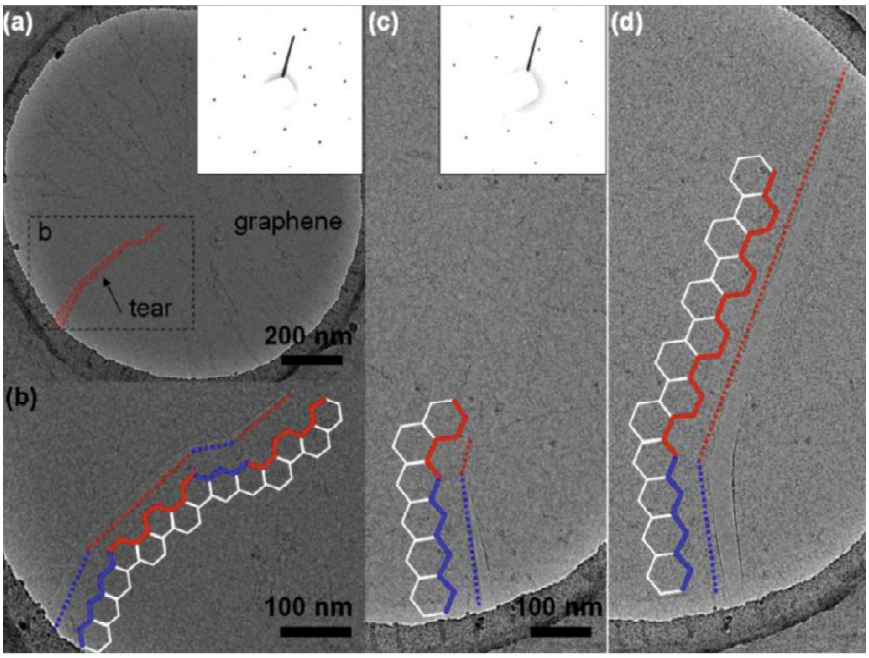

Fig. 2. Tears in a suspended graphene membrane. (a) TEM image of suspended graphene transferred to a Quantifoil holey carbon TEM grid with a tear near the edge of the carbon support. The inset is the rotation-calibrated diffraction pattern of graphene. The dashed rectangle is the field of view for panel b. (b) Zoomed-in TEM image of the tear in graphene. The tear exhibits straight lines with the direction occasionally changing by 30°. The red and blue dotted lines represent armchair and zigzag tear edges, respectively. (c) TEM image of a graphene tear before the propagation. The inset is the rotation-calibrated diffraction pattern of graphene membrane. (d) Propagated tear in graphene under electron beam. The freshly torn line is straight following the armchair direction of the graphene lattice. Reprinted with permission from [K. Kim, V.I. Artyukhov, W. Regan, Y. Liu, M.F. Crommie, B.I. Yakobson, A. Zettl, Ripping graphene: Preferred directions. *Nano Letters*, Volume ***12***, 293-297 (2012)]. Copyright (2012) by American Chemical Society.

break in the vicinities of tear tips, providing the experimentally observed tear propagation.

Similar crystallographic features of cracks/tears were observed in computer simulations focused on tearing/exfoliation of graphene sheets from adhesive substrates [11]. These simulations were motivated by the experimentally documented fact (see [11] and references therein) that graphene ribbons produced by the tearing/exfoliation processes typically have tapered geometry (Fig. 3), with the angles of tear being sensitive to the adhesion substrate. Following the discussed computer simulations in the case of comparatively low adhesion strengths, the tearing mechanism represents growth of tears along a dominant armchair direction of the hexagonal crystal lattice of graphene with occasional changes providing rarely distributed small zigzag ledges at the armchair tear edges (Figs. 4a and 4b). This crystallography of tear growth leads to the tapered geometry of the resultant graphene ribbons with low tear angles. In the case of comparatively high adhesion strengths, changes of tear growth direction by 60° come into play (Figs.

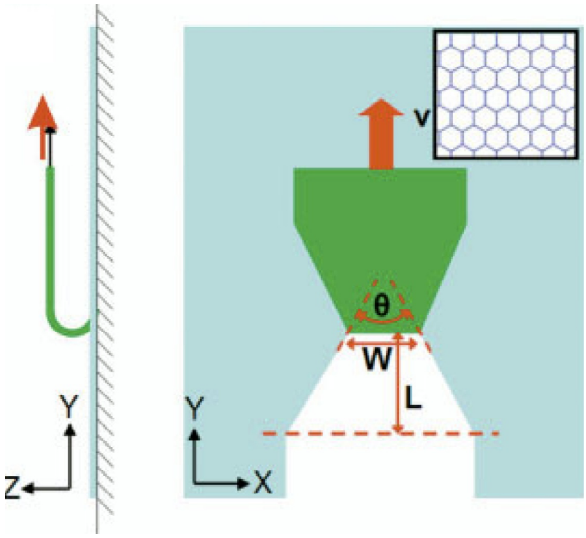

Fig. 3. Schematic diagram of the setup for the tearing studies of graphene: side and top views. The inset shows the sheet orientation. An initial flap of 8 nm in width is cut in the sheet, folded back, and moved at a constant speed. Reprinted with permission from [D. Sen, K.S. Novoselov, P. Reis, M.J. Buehler, *Small*, Volume **6**, 1108 (2010)]. Copyright (2010) by John Wiley and Sons.

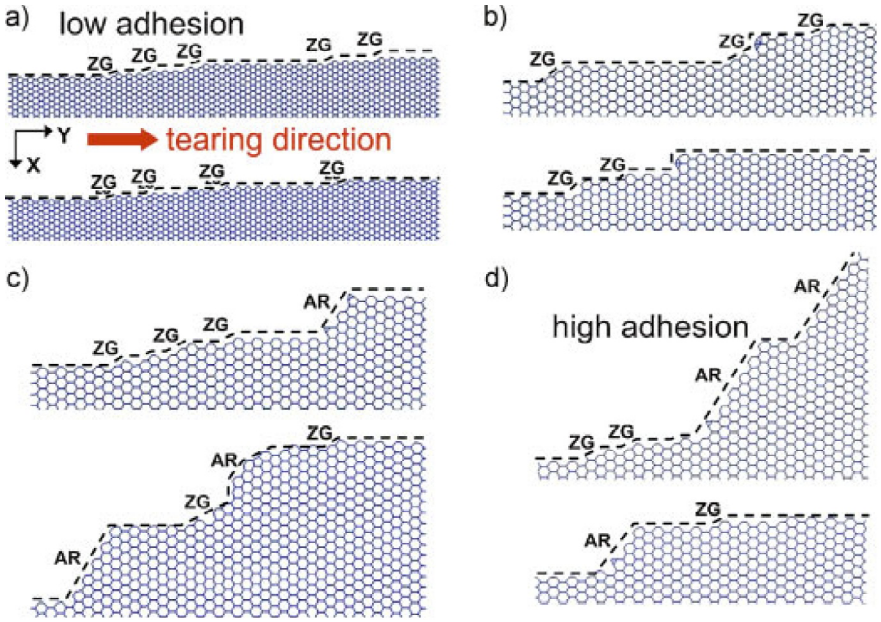

Fig. 4. Atomistic tearing mechanisms for different adhesion strengths and edge geometries for the two edges formed as the tear moves forward. The two subfigures in each panel represent shape of the two crack lips formed on either side of the tearing ridge. Results are shown for adhesion strengths of (a) 2.4, (b) 14.3, (c) 16.7, and (d) 20.2 J m^{-2}. At lower adhesion strengths ((a) and (b)), the fracture surface largely consists of first-armchair edges (unlabeled, horizontal dotted lines) with small zigzag ledges (marked as ZG) that provide the geometric means that reduce the width of the torn sheet. At higher adhesion strengths ((c) and (d)), the second armchair edge begins to form (marked as AR) and takes over large sections of the torn sheet. Reprinted with permission from [D. Sen, K.S. Novoselov, P. Reis, M.J. Buehler, *Small*, Volume **6**, 1108 (2010)]. Copyright (2010) by John Wiley and Sons.

4c and 4d). As a corollary, each tear has its edges with two dominant armchair directions in parallel with small zigzag ledges, and this crystallography results in the tapered geometry of the graphene ribbons with comparatively high tear angles. The tearing mechanisms under consideration (Fig. 4) are well consistent with the corresponding experimental data.

3. DISLOCATIONS AND GRAIN BOUNDARIES IN GRAPHENE

The presence of defects in graphene is capable of significantly or even crucially influencing its plastic deformation and fracture. Typical defects experimentally observed in graphene are vacancies [12], Stone-Wales defects [12], dislocations [13] and grain boundaries (GBs) composed of dislocations (Figs. 5 and 6) [14-17]. Dislocations and GBs in graphene cause the most significant effects on its mechanical properties. In particular, dislocations can serve as carriers of plastic flow in graphene [13,18], whereas GBs dramatically decrease its strength characteristics [14,19].

Perfect lattice dislocations in graphene are point defects violating its translational symmetry [13,17-23]. They represent pentagon-heptagon pairs in 2D hexagonal crystal lattice (see, e.g., Figs. 5 and 6 where dislocations are shown as structural blocks of GBs). Perfect dislocations are characterized by Burgers vectors $\boldsymbol{b}$ being lattice vectors of hexagonal crystal. Any Burgers vector $\boldsymbol{b}$ of a perfect dislocation admits decomposition into the basic vectors, $\boldsymbol{a}_1$ and $\boldsymbol{a}_2$, of 2D hexagonal crystal lattice. In doing so, lattice dislocations have Burgers vectors $\boldsymbol{b} = m\boldsymbol{a}_1 + n\boldsymbol{a}_2$, with m and n being integers, and are often called (m,n)-dislocations [17-23].

Plastic deformation in conventional 3D solids occurs mostly through generation and motion of lattice dislocations. In the context discussed, of utmost interest is the recent experimental observation of generation and motion of lattice dislocations in graphene under electron beam irradiation [13]; see also discussion in Ref. [18]. As it has been demonstrated in the experiment [13], a dipole of lattice dislocations is generated in graphene, and dislocations glide and climb in a graphene sheet which thereby is locally deformed. These experimental results on electron beam induced evolution of dislocations form a basis for understanding the nature of dislocation plasticity in graphene and motivate its further examinations.

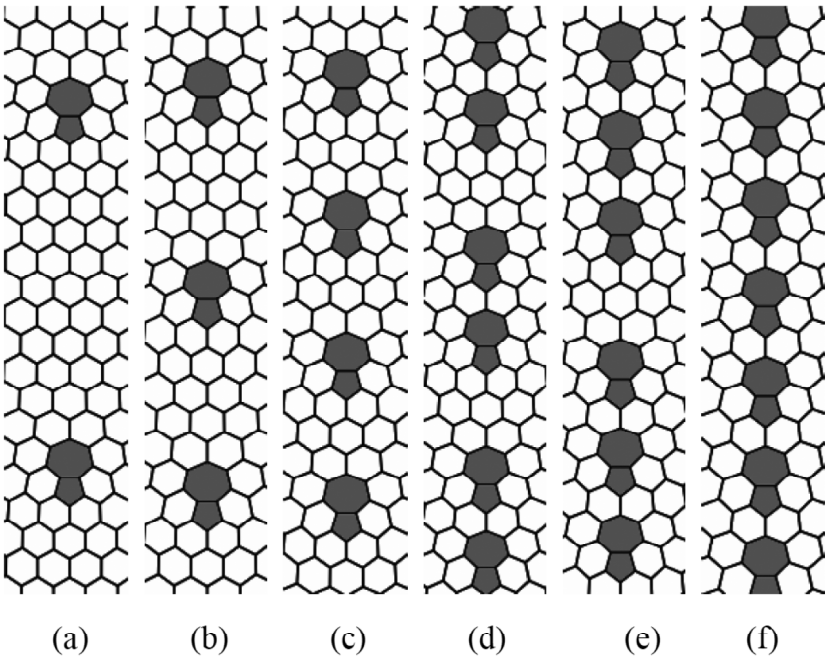

Fig. 5. The dislocation structures of armchair GBs at six grain misorientation angle θ (a) θ = 5.1°, (b) θ = 9.5°, (c) θ = 13.2°, (d) θ = 16.4°, (e) θ = 17.9°, and (f) θ = 21.8°. Reprinted with permission from [Y. Wei, J. Wu, H. Yin, X. Shi, R. Yang, M. Dresselhaus, The nature of strength enhancement and weakening by pentagon-heptagon defects in graphene. *Nature Materials,* Volume **11**, 759 (2012)]. Copyright (2012) by Nature Publishing Group.

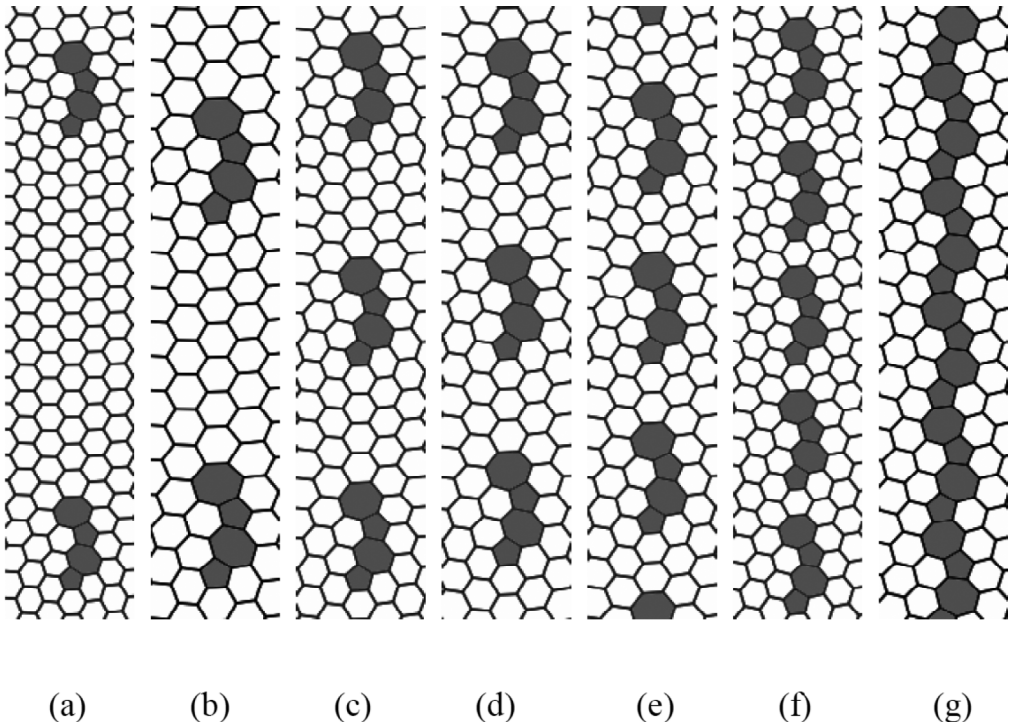

Fig. 6. The dislocation structures of zigzag GBs at seven grain misorientation angle θ (a) θ = 5.7°, (b) θ = 9.5°, (c) θ = 13.2°, (d) θ = 15.2°, (e) θ = 17.9°, (f) θ = 21.8°, and (g) θ = 27.8°. Reprinted with permission from [Y. Wei, J. Wu, H. Yin, X. Shi, R. Yang, M. Dresselhaus, The nature of strength enhancement and weakening by pentagon-heptagon defects in graphene. *Nature Materials,* Volume **11**, 759 (2012)]. Copyright (2012) by Nature Publishing Group.

Now let us turn to discussion of GBs in graphene. GBs by definition are line defects separating graphene grains (crystallites/domains) with different crystal lattice orientations (Figs. 5 and 6). More precisely, each GB in a 2D graphene sheet separates two 2D grains whose crystal lattices are rotated/tilted relative each other by a tilt misorientation angle θ (characterizing the boundary), with the rotation axis being perpendicular to the sheet plane. A GB is called symmetric, if orientations of crystal lattices of its adjacent grains relative to the boundary line are symmetric, and asymmetric otherwise [17,21-23].

According to experimental data, computer simulations and theoretical models, low- and high-angle GBs in graphene hexagon lattices are represented as walls of topological edge dislocations or, in other terms, pentagon-heptagon pairs (Fig. 3) [14-17, 19, 21-28]. In doing so, geometry of a GB is specified by Burgers vectors and core structures of GB dislocations as well as by parameters of dislocation wall arrangement. Typical dislocations composing GBs in graphene are (1,0)–dislocations (Fig. 5) and pairs of (1,0)- and (0,1)-dislocations (Fig. 6). The (1,0)–dislocation core contains edge-sharing heptagon-pentagon pair called also the armchair configuration, and GBs composed of (1,0)–dislocations are called armchair GBs (Fig. 5). A pair of (1,0)- and (0,1)-dislocations is characterized by the sum Burgers vector (1,1) and has a zigzag core configuration consisting of two heptagon-pentagon pairs, as it is shown in Fig. 6. GBs composed of such dislocation pairs are called zigzag GBs (Fig. 6).

In analytical examinations and computer simulations, symmetric GBs are modeled as periodic straight walls composed of identical dislocations [21-27]. Real GBs in graphene specimens are not strictly periodic and typically have serpentine-like geometry [14-16,19].

Recently, migration of a GB composed of dislocations has been experimentally observed in graphene [29]. The GB migration process occurs through motion of GB dislocations [28], and this experimentally documented fact indirectly indicates in favor of representations [13,18] on important role of dislocations in carrying plastic flow in graphene.

4. EFFECTS OF GRAIN BOUNDARIES ON MECHANICAL PROPERTIES OF GRAPHENE

Recently, large-area polycrystalline graphene sheets have been produced to meet technological needs; see, e.g., [30,31]. GBs serve as inevitable structural elements in large-area graphene specimens, and thereby their effects on the mechanical properties of graphene are very interesting from both fundamental and applied viewpoints. Following experimental data [14], the failure strength of free-standing polycrystalline graphene under concentrated mechanical load dramatically degrades compared to that of its single-crystal counterpart. In the experiment under consideration, a polycrystalline graphene membrane was loaded by tip of atomic force microscope. It was found that the graphene tears along GBs at load of ≈100 nN [14]. This value is an order of magnitude lower than typical values (≈1.7 mN) specifying fracture of single-crystal exfoliated graphene [5].

Also, strength characteristics of polycrystalline graphene have been examined in atomic force nanoindenation experiment and molecular dynamics simulations [19] with focuses placed on the effects of GBs and nanoscale out-of-plane rippling. In this experiment, polycrystalline graphene specimens were grown by chemical vapor deposition method on copper substrate and then transferred onto silicon nitride grids with arrays of prepatterned holes. GBs were experimentally identified as lines where enhanced absorption of amorphous carbon and iron oxide nanoparticles occurs [19]. The nanoindentation experiment [19] showed that GBs and out-of-plane ripples effectively decrease the strength of polycrystalline graphene. For instance, according to a series of nanoindentation measurements of graphene membranes [19], the upper bound for the in-plane breaking stress is of ≈35 GPa, and this value is much lower than the intrinsic strength (≈130 GPa) of pristine graphene [5]. Besides, the experimentally documented value of ≈35 GPa [19] is lower than those (50-100 GPa) revealed in computer simulations of strength exhibited by graphene bi-crystals with various GB structures [23-27]. In order to explain the discrepancy between the experiment and simulations, Ruiz-Vargas with coworkers [19] assumed the existence of nanovoids at real GBs in polycrystalline graphene membranes. With this assumption, molecular dynamics simulations were performed with focuses placed on strength exhibited by graphene polycrystals containing nanovoids at GBs. According to the simulations, the presence of nanovoids at GBs leads to a dramatic decrease in the strength characteristics of graphene bi-crystals and make them consistent with the reported experimental data [19].

Strength characteristics of graphene bi-crystals were examined by several groups in computer simulations [23-27]. The key focuses were placed on sensitivity of the tensile strength to GB misorientation depending on a periodic GB dislocation structure. For instance, the tests in the simulations [24] were performed with graphene sheets pulled perpendicular and parallel to GB lines. For these load geometries in the cases of armchair and zigzag GBs, computer simulations [24] show the trend that, as the GB misorientation increases, both the ultimate failure strength and strain at failure grow. In particular, it was found that graphene sheets containing high-angle GBs (specified by misorientatioin angles close to 20° - 30°) with dense dislocation structures have strength values exceeding those of graphene sheets containing low-angle GBs with low-density dislocation structures [24]. Similar trends have been reported by other groups [23,25-27] on the basis of their computer simulations.

From a physical viewpoint, fracture in a graphene bi-crystal starts as a break of an atomic bond at which the normal stress σ_{xx} (defined/calculated as the superposition of the external tensile stress and the normal stress created by dislocations composing a GB) reaches its maximum value [23,24]. Within the discussed interpretation, local strains created by low-density, large-period dislocation structures of low-angle GBs in graphene (see, e.g., Figs. 5 (a and b) and 6 (a and b)) are higher than those created by high-density, small-period dislocation configurations composing high-angle GBs (see, e.g., Figs. 5f and 6 (f and g)). (This statement follows from the standard theory of dislocation walls in solids [6] and is supported by analytical calculations [23].) That is, local strains at critical bonds in the case of low-angle boundaries are high enough to initiate failure at lower level of the applied external stress, compared to the case of high-angle GBs.

The simulations [23] revealed some deviations from the previously reported [24] monotonic decrease in strength with growing the tilt GB misorientation angle θ. More precisely, Wei with co-workers [23] showed that strength of bi-crystals with armchair GBs increases, decreases and increases again with rising θ (Fig. 7). The non-monotonic character of the $\sigma(\theta)$ dependence (Fig. 7) is logically attributed to sensitivity of the equilibrium armchair GB structure (minimizing GB energy) to θ. With this sensitivity, analytical calculations [23] in the case of armchair GBs demonstrated that the maximum normal stress σ_{xx} appears in the bond shared by hexagon-heptagon rings, which increases,

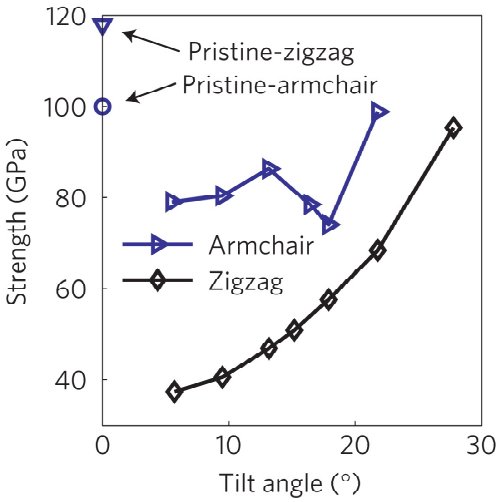

Fig. 7. GB normal strength as a function of tilt angle. The two isolated points are the strengths of pristine graphene stretching in zigzag ('open down triangle') and armchair ('open circle') directions, respectively. Reprinted with permission from [Y. Wei, J. Wu, H. Yin, X. Shi, R. Yang, M. Dresselhaus, The nature of strength enhancement and weakening by pentagon-heptagon defects in graphene. *Nature Materials,* Volume **11**, 759 (2012)]. Copyright (2012) by Nature Publishing Group.

decreases and increases again with increasing θ. The analytical results are well consistent with the computer simulations [23].

Jhon with co-workers [26] presented results of molecular dynamics simulations focused on mechanical characteristics of graphene bicrystals under tension and compression tests in directions perpendicular and parallel to GBs. They found several remarkable specific features of deformation and fracture processes in graphene sheets containing GBs. First, tension in the direction perpendicular to GBs initiates incomplete fracture resulting in formation of long monatomic carbon chains between two large fragments of a deformed specimen (Fig. 8). The incomplete fracture stage is specified by dramatic decrease in the slope and a rugged pattern in the stress-strain curves. Jhon with co-workers [26] noted that the incomplete fracture process can be viewed as a new methodology for fabrication of long monatomic carbon chains being of both fundamental interest and potential significance for electronics. Second, fracture starts from breaking of atomic bonds at heptagons in heptagon-hexagon pairs and occurs through the generation and growth of nanovoids at such pairs. That is, several nanovoids are almost simultaneously generated and then gradually evolve as carriers of nanoscale fracture

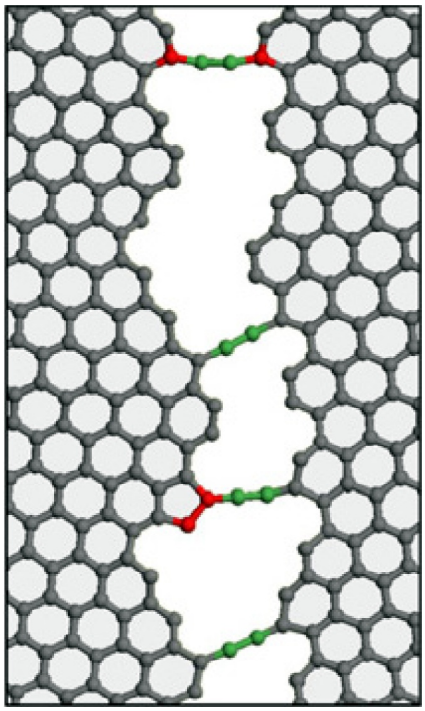

Fig. 8. The production of monatomic carbon chains by elongation of graphene bi-crystal in direction perpendicular to pre-existent grain boundary [26]. Reproduced from [26] with permission of PERGAMON in the format reuse in a journal/ magazine via Copyright Clearance Center. Copyright (2012) by PERGAMON.

in graphene bicrystals. This fracture behavior is different from that (generation and catastrophic growth of one crack in a specimen) of pristine graphene.

Also, following [26], graphene sheets with parallel GBs show specific behavioral features in compression tests. In particular, bending of a graphene sheet is enhanced along GB lines when the sheet is compressed perpendicular to GBs. This feature can be exploited in design of polycrystalline graphene specimens with tuned folded structures affecting both their transport and mechanical characteristics. Besides, according to the simulations [26], compression parallel to GBs produces complicatedly arranged, spatially inhomogeneous folded structures, and this feature is also interesting for design of nanodevices based on folded graphene specimens.

Recently, it has been revealed that elastic strains generated in moderately curved graphene structures such as bubbles and balloons strongly influence the excellent electronic properties of graphene; see theoretical models [32-35] and experimental data [36-38]. This opens a technologically important opportunity to design and control electronic properties of graphene sheets through their curvature characteristics. More than that, various carbon allotropes (like fullerenes, cones, capped carbon nanotubes, etc.) can be viewed as those produced by insertion of topological disclinations, first of all, pentagons into mature, single crystalline graphene; see, e.g., [2,17,22,39-42]. Also, following [17], formation of partial GB disclinations in polycrystalline graphene can be effectively exploited in fabrication and design of both weakly curved graphene specimens and new curved carbon nanostructures whose electronic characteristics are sensitive to curvature. (In doing so, partial disclinations at a GB in graphene are defined [17] as point defects at which the GB changes its misorientation in a step-like manner. They represent point analogs of line, partial GB disclinations in conventional 3D nanocrystalline solids [43-46].) In the context discussed, there is large interest in experimental characterization, computer simulations and theoretical analysis of mechanical properties exhibited by curved, disclinated graphene sheets and new curved carbon nanostructures with partial GB disclinations.

In addition, partial GB disclinations in graphene [17] can significantly enhance crack nucleation and thereby influence graphene' strength. This aspect is worth being taken into account in explanation of the discrepancy between experimental measurements [14,19] and simulations [23-27] of strengths characterizing polycrystalline graphene sheets.

5. MECHANICAL PROPERTIES OF COMPOSITES WITH GRAPHENE INCLUSIONS

Due to ultrahigh strength of graphene, its inclusions are effectively used in enhancement of both strength and fracture toughness in composite materials [47-54]. For instance, in order to improve fracture toughness of ceramic materials, several research groups fabricated nanocomposites consisting of ceramic matrixes and inclusions in the form of graphene platelets (GPLs); see, e.g., [47,48]. In particular, Kvetkova with coworkers [48] fabricated silicon nitride + 1 wt.% GPL nanocomposites with relatively homogeneously dispersed GPLs. Each GPL consists of several graphene layers and has thickness of approximately 1-10 nm and length and width of approximately 0.05 – 10 microns. The nanocomposites with GPLs exhibit a pronounced enhancement in the fracture toughness with the highest value of K_{IC} = 9.92 MPa m$^{1/2}$ [38], compared to the toughness (K_{IC} = 6.89 MPa m$^{1/2}$) of mono-

lithic silicon nitride without GPLs. The dominant toughening mechanisms are found to be crack branching, crack deflection and crack bridging. Besides, it was noted that use of GPLs as nanoinclusions in ceramic-matrix composites is more effective in their toughening than that of carbon nanotubes and/or carbon nanofibers [48].

Also, inclusions in the form of graphene sheets provide enhancement of mechanical characteristics in polymer-based nanocomposites [49-54]. For instance, partially oxiginated graphene sheets were dispersed in polymer matrix, and mechanical characteristics of resultant nanocomposites with various graphene contents were examined [50]. It was experimentally found that the mode I fracture toughness (K_{IC}), the ultimate tensile strength and Young modulus of the nanocomposite with 0.125% weight fraction of graphene inclusions are by 65%, 45%, and 50% larger than those of its graphene-free counterpart (the baseline epoxy), respectively. On the basis of fractography analysis, Rafiee with coworkers [50] attributed the experimentally documented dramatic enhancement of toughness to the role of dispersed graphene sheets as hard inclusions that deflect growing cracks and thus increase both fracture surface roughness and its energy. Besides, crack deflection due to graphene inclusions in the nanocomposites locally provide mixed-mode conditions for growing cracks, and this factor also hampers crack growth compared to pure mode I conditions.

The fracture toughness K_{IC} of the graphene-polymer nanocomposite as a function of the graphene weight fraction W has its maximum at $W = 0.125\%$, and K_{IC} gradually decreases with further increase in W [50]. Rafiee with coworkers relate this behavior to degradation in the dispersion of graphene sheet inclusions at $W > 0.125\%$. Note that the 65% increase in the fracture toughness of an epoxy system due to addition of graphene inclusions at $W = 0.125\%$ is remarkable in the sense that a similar level of increase in the fracture toughness can be achieved by insertion of other inclusions, but at much higher weight fractions of these inclusions. For instance, one can increase the fracture toughness by around 60-65% through addition of SiO_2 at its $W = 14.8\%$ [55], Al_2O_3 at the volume fraction of $\approx 5\%$ [56], and TiO_2 at the volume fraction of $\approx 10\%$ [56]. Also, the 42% increase in the fracture toughness is achieved by addition of carbon nanotubes at $W \approx 0.5\%$ [57]. The discussed advantage of graphene sheets as toughening inclusions in polymer-based nanomposites is logically attributed to its sheet geometry that is more effective in crack deflection, compared to ball-like and cylinder-like shapes of $SiO_2/Al_2O_3/TiO_2$ nanoparticles and carbon nanotubes, respectively. In addition, since degradation in the dispersion of graphene sheet inclusions at high enough values of W leads to suppression of their toughening effect, a more homogeneous dispersion of such inclusions may dramatically enhance the fracture toughness of polymer-graphene nanocomposites at $W > 0.125\%$.

To summarize, the experimental data [47-54] are indicative of very promising role of graphene inclusions (sheets, platelets) as strengthening and toughening structural elements in nanocomposites. In doing so, graphene inclusions can be more effective compared to nanoparticles and carbon nanotubes.

6. CHALLENGES

Studies of mechanical properties exhibited by graphene are in their infancy. Therefore, in this new and intriguing research area, there are many important unsolved problems. In particular, the following challenges are of crucial interdisciplinary significance:

(A) Unambiguous experimental identification, computer modeling and theoretical description of the fundamental effects caused by vacancies, dislocations and GBs on mechanical properties (strength, plasticity, toughness, etc.) of graphene.

(B) With (A) used as an input, fabrication of flat and weakly curved graphene specimens with geometric and structural parameters that control, enhance and design the mechanical properties of graphene.

(C) Search for new carbon nanostructures as highly curved polycrystalline graphene specimens (containing partial GB disclinations) and examinations of their mechanical properties.

(D) Development of novel experimental methods and techniques for characterization of mechanical properties of graphene.

(E) Unambiguous experimental identification, computer modeling and theoretical description of the fundamental effects caused by nanoscale graphene inclusions in ceramic-, metal- and polymer-based nanocomposites on their mechanical properties.

(F) Fabrication of 2D graphene-matrix nanocomposites with chemically distinguished 2D inclusions of other phases and studies of their mechanical properties.

(G) Search for new hybrid carbon nanomaterials - nanocomposites structurally composed of graphene

and other carbon allotropes - and studies of their mechanical properties.

Success in treatment of these important unresolved questions will make a large impact on fundamental science of graphene and open new intriguing perspectives in fabrication and applications of both graphene and new curved carbon nanostructures with the outstanding mechanical properties.

ACKNOWLEDGEMENTS

This work was supported in part by the Ministry of Education and Science of the Russian Federation (Contract 8025) and the Russian Foundation of Basic Research (grant 12-01-00291-à).

REFERENCES

[1] K.S. Novoselov, A.K. Geim, S.V. Morozov, D. Jiang, Y. Zhang, S.V. Dubonos, I.V. Grigorieva and A.A. Firsov // *Science* **306** (2004) 666.

[2] A.K. Geim and K.S. Novoselov // *Nature Mater*. **6** (2007) 183.

[3] A.K. Geim // *Science* **324** (2009) 1530.

[4] A.H. Castro Nero, F. Guinea, N.M.R. Peres, K.S. Novoselov and A.K. Geim // *Rev. Mod. Phys*. **81** (2009) 109.

[5] C. Lee, X. Wei, J.W. Kysar and J. Hone // *Science* **321** (2008) 385.

[6] J.P. Hirth and J. Lothe, *Theory of Dislocations*. (Wiley, New York, 1982).

[7] C.C. Koch, I.A. Ovid'ko, S. Seal and S. Veprek, *Structural Nanocrystalline Materials: Fundamentals and Applications* (Cambridge University Press, Cambridge, 2007).

[8] T. Zhu and J. Li // *Progr. Mater. Sci.* **55** (2010) 710.

[9] F. Liu, P. Ming and J. Li // *Phys. Rev. B* **76** (2007) 064120.

[10] K. Kim, V.I. Artyukhov, W. Regan, Y. Liu, M.F. Crommie, B.I. Yakobson and A. Zettl // *Nano Lett.* ***12*** (2012) 293.

[11] D. Sen, K.S. Novoselov, P. Reis and M.J. Buehler // *Small* **6** (2010) 1108.

[12] J.C. Meyer, C. Kisielowski, R. Erni, M.D. Rossell, M.F. Gommie and A. Zettl // *Nano Lett.* **8** (2008) 3582.

[13] J.H. Warner, E.R. Margine, M. Mukai, A.W. Robertson, F. Guistino and A.I. Kirkland // *Science* **337** (2012) 209.

[14] P. Y. Huang, C.S. Ruiz-Vargas, A. M. van der Zande, W.S. Whitney, M.P. Levendorf, J.W. Kevek, S. Garg, J.S. Alden, C.J. Hustedt, Y. Zhu, J. Park, P.L. McEuen and D.A. Muller // *Nature* **469** (2011) 389.

[15] K. Kim, Z. Lee, W. Regan, C. Kisielowski, M.F. Gommie and A. Zettl // *ACS Nano* **5** (2011) 2142.

[16] Q. Yu, L.A. Jauregui, W. Wu, R. Colby, J. Tian, Z. Su, H. Cao, Z. Liu, D. Pandey, D. Wei, T.F. Chung, P. Peng, N.P. Guisinger, E.A. Stach, J. Bao, S.-S. Pei and Y.P. Chen // *Nature Mater*. **10** (2011) 443.

[17] I.A. Ovid'ko // *Rev. Adv. Mater. Sci*. **30** (2012) 201.

[18] L.L. Bonilla and A. Carpio // *Science* **337** (2012) 161.

[19] C.S. Ruiz-Vargas, H.L. Zhuang, P.Y. Huang, A.M. van der Zande, S. Garg, P.L. McEuen, D.A. Miller, R.C. Hennig and J. Park // *Nano Lett*. **11** (2011) 2259.

[20] A. Carpio, L.L. Bonilla, F. de Juan and M.A.H. Vozmediano // New J. Phys. **10** (2008) 053021.

[21] O.V. Yazyev and S. Louie // *Phys. Rev. B* **81** (2010) 195420; *Nature Mater*. **9** (2010) 806.

[22] Y. Liu and B.I. Yakobson // *Nano Lett*. **10** (2010) 2178.

[23] Y. Wei, J. Wu, H. Yin, X. Shi, R. Yang and M. Dresselhaus // *Nature Mater*. **11** (2012) 759.

[24] R. Grantab, V.B. Shenoy and R.S. Ruoff // *Science* **330** (2010) 946.

[25] T.-H. Liu, C.-W. Pao and C.-C. Chang // *Carbon* **50** (2012) 3465.

[26] Y.I. Jhon, S.-E. Zhu, J.-H. Ahn and, M.S. Jhon // *Carbon* **50** (2012) 3708.

[27] J. Zhang, J. Zhao and J. Lu // *ACS Nano* **6** (2102) 2704.

[28] P.M. Ajayan and B.I. Yakobson // *Nature Mater*. **10** (2011) 415.

[29] S. Kurasch, J. Kotakowski, O. Lehtinen, V. Skakalova, J. Smet, C.E. Krill III, A.V. Krasheninnikov and U. Kaiser // *Nano Lett*. **12** (2012) 3168.

[30] K.V. Emtsev, A. Bostwick, K. Horn, J. Jobst, G.L. Kellogg, L. Ley, J.L. McChesney, T. Ohta, S.A. Reshanov, J. Rohl, E. Rotenberg, A. Schmid, D. Waldmann, H.B. Weber and T. Seyller // *Nature Mater*. **8** (2009) 203.

[31] K.S. Kim, Y. Zhao, H. Jang, S.Y. Lee, J.M. Kim, K.S. Kim, J.-H. Ahn, P. Kim, J.-Y. Choi and B.H. Hong // *Nature* **457**, 706 (2009).

[32] V.M. Pereira and A.H. Castro Neto // *Phys. Rev. Lett.* **103** (2009) 046801.

[33] V. Atanasov and A. Saxena // *Phys. Rev. B* **81** (2010) 205.
[34] V. Atanasov and A. Saxena // *J. Phys.: Condens. Matter* **23** (2011) 175301.
[35] F. Guinea, M.I. Katsnelson and A.K. Geim // *Nature Phys.* **6** (2011) 30.
[36] N. Levy, S.A. Burke, K.L. Meaker, M. Panlasigui, A. Zettl, F. Guinea, A.H. Castro Neto and M.F. Grommie // *Science* **329** (2010) 544.
[37] T. Georgiou, L. Britnell, P. Blake, R.V. Gorbachev, A. Gholinia, A.K. Geim, C. Casiraghi and K.S. Novoselov // *Appl. Phys. Lett.* **99** (2011) 093103.
[38] J. Zabel, R.R. Nair, A. Ott, T. Georgiou, A.K. Geim, K.S. Novoselov and C. Casiraghi // *Nano Lett.* **12** (2012) 617.
[39] S. Ihara, S. Itoh, K. Akagi, R. Tamura and M. Tsukada // *Phys. Rev. B* **54** (1996) 14713.
[40] S. Gupta and A. Saxena // *J. Appl. Phys*. **109** (2011) 074316.
[41] S. Gupta and A. Saxena // *J. Appl. Phys*. **112** (2012) 114316.
[42] I.A. Ovid'ko // *Rev. Adv. Mater. Sci*. **32** (2012) 1.
[43] I.A. Ovid'ko // *Science* **295** (2002) 2386.
[44] M. Kleman and J. Friedel // *Rev. Mod. Phys.* **80** (2008) 61.
[45] S.V. Bobylev, N.F. Morozov and I.A. Ovid'ko // *Phys. Rev. Lett*. **105** (2010) 055504; *Phys. Rev. B* **84** (2011) 094103.
[46] S.V. Bobylev and I.A. Ovid'ko // *Phys. Rev. Lett*. **109** (2012) 175501.
[47] L.S. Walker, V.R. Marotto, M.A. Rafiee, N. Koretkar and E.L. Corral // *ACS Nano* **5** (2011) 3182.
[48] L. Kvetkova, A. Duszova, P. Hvizdos, J. Dusza, P. Kun and C. Balazsi // *Scr. Mater*. **66** (2012) 793.
[49] J. Liang, Y. Huang, L. Zhang, Y. Wang, Y. Ma, T. Guo and Y. Chen // *Adv. Funct. Mater.* **19** (2009) 2297.
[50] M.A. Rafiee, J. Rafiee, I. Srivastana, Z. Wang, H. Song, Z.-Z. Yu and N. Koratkar // *Small* **6** (2010) 179.
[51] X. Zhao, Q. Zhang and D. Chen // *Macromolecules* **43** (2010) 2357.
[52] T. Kuilla, S. Bhadha, D. Yao, N.H. Kim, S. Bose and J.H. Lee // *Prog. Polymer. Sci.* **35** (2010) 1350.
[53] Q. Xu, Y. Gong, Y. Fang, G. Jiang, Y. Wang, X. Sun and R. Wang // *Bull. Mater. Sci*. **35** (2012) 795.
[54] P. May, U. Khan, A. O'Neill and J.N. Coleman // *J. Mater. Chem*. **22** (2012) 1278.
[55] B.R.K. Blackman, A.J. Kinloch, J. Sohn Lee, A.C. Taylor, R. Agarwal, G. Schueneman and S. Sprenger // *J. Mater. Sci*. **42** (2007) 7049.
[56] B. Wetzel, P. Rosso, F. Haupert and K. Friedrich // *Eng. Fract. Mech*. **73** (2006) 2375.
[57] F.H. Goiny, M.H.G. Wichmann, B.K. Fiedler and K. Schulte // *Comp. Sci. Technol.* **65** (2005) 2300.